JOURNAL OF MATERIALS SCIENCE **33** (1998) 5131–5136

Supersolidus liquid phase sintering of moulded metal components

J. L. CHAN, J. R. ALCOCK, D. J. STEPHENSON
School of Industrial and Manufacturing Science, Cranfield University, Cranfield, Bedfordshire, MK43 0AL, UK
E-mail: j.r.alcock@cranfield.ac.uk

The influence of supersolidus liquid phase sintering (SLPS) on the density of sintered components manufactured using a Ni-base superalloy powder (N18) has been studied. A compression moulding technique was employed to simulate the metal injection moulding (MIM) process using coarse N18 powder, with a particle size distribution of 40–63 μm, as opposed to fine powders of less than 10 μm normally used in conventional MIM. The study has demonstrated how the problem of low sintered density, encountered in solid-state sintering using coarse powders, can been overcome by SLPS and that the sintered densities of the N18 powder via the moulding process route were comparable with those produced by conventional die pressing and sintering. © *1998 Kluwer Academic Publishers*

1. Introduction

Among the recent developments in powder metallurgy (PM), metal injection moulding (MIM) is a promising process for producing near-net-shape components. MIM is generally composed of four steps: mixing of metal powder and binders, moulding, debinding and sintering [1]. Even though the MIM process for forming near-net-shape PM parts is becoming increasingly popular, a disadvantage of the process is the requirement for powders to possess a small mean particle size ($<10\ \mu$m) in order to achieve near theoretical density of the final part following sintering. Owing to the high cost of fine powders, one way to make the MIM process more economical would be to utilize coarse powders. However, to solve the problem of reduced densification rates during sintering resulting from using coarse powders, enhanced sintering processes must also be introduced.

One promising approach to sintering with coarse powders is supersolidus liquid phase sintering (SLPS) [2]. In SLPS, pre-alloyed powders are heated to a temperature between their solidus and liquidus to obtain partial melting. Densification then occurs by a mixture of capillary rearrangement (grain sliding) and solution-reprecipitation. The significantly reduced time for sintering makes SLPS using coarse powders relatively economical. Theoretical models of the debinding of MIM parts predict that a secondary benefit of using coarser particles would be a reduction in debinding time [3], again enhancing the ease and economics of the MIM process.

2. Experimental procedure

Two experimental routes were investigated to produce sintered specimens from a relatively coarse Ni-base superalloy powder. In the first route, powders were die pressed to form 20 mm diameter discs, which were sintered in a vacuum furnace. The second route was that of compression moulding the superalloy powder mixed with a MIM binder system. This was used to simulate the MIM process, as currently available standard injection moulding machines have too small a screw-barrel clearance to enable satisfactory moulding using large powder particles. The compression moulded discs were subsequently debound and sintered following a well established MIM process cycle. The sintered densities obtained from both experimental routes were correlated to determine whether the coarse pre-alloyed powders were suitable for use in an injection moulding process to manufacture complex parts.

2.1. Powder characterization

A commercial Ni-base superalloy N18 (Imphy S.A.) was used in this study. The composition is listed in Table I. This PM alloy is strengthened by a high volume fraction of γ' (55%) and was designed for applications in a high temperature turbine disc [4].

The morphology of the as-received N18 powder, with a nominal particle size range of 15–110 μm, was examined using scanning electron microscopy and is shown in Fig. 1. The particle size distribution of the as-received powder was characterized by sieving and the powder was separated into three sub-batches of particle size range 15–40, 40–63 and 63–110 μm.

Differential thermal analysis (DTA) was used to determine the percentage of liquid formed in the N18 powder as a function of temperature. A differential scanning calorimeter (DSC1500), with a thermal analysis software system (Plus V software), was utilized for the DTA measurements.

TABLE I Chemical composition (wt %) of N18

Ni	C	Co	Cr	Mo	Al	Ti	B	Hf	Zr	O	N
Balance	0.015	15.7	11.5	6.5	4.35	4.35	0.015	0.45	0.03	$\leq$0.010	$\leq$0.005

TABLE II Binder system components and their properties

Component	Density ($g\,cm^{-3}$)	Molecular weight ($g\,mol^{-1}$)	Melting temperature ($^{\circ}C$)
LMW polypropylene	0.903	43 000	170
Carnauba wax	0.970	1300–1500	84
Paraffin wax	0.900	350–420	59
Stearic acid	0.941	285	74

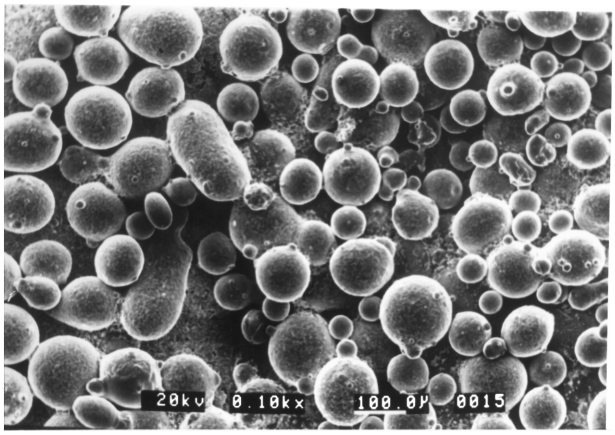

Figure 1 SEM micrograph of the as-received argon atomized N18 powder.

2.2. Compression moulding

For compression moulding, N18 powder with a particle size range of 40–63 μm was investigated. A binder system for plastic forming was selected, which allowed a two stage binder removal process; solvent and thermal debinding. The binder system consisted of low molecular weight polypropylene, paraffin wax and carnauba wax. Details of the binder components are summarized in Table II. Previous research [5] has shown that the relatively low polypropylene content may result in green components being brittle and exhibiting a low green strength after moulding. Accordingly, the binder system used in this study was: polypropylene, 60 wt %; paraffin wax, 32.6 wt %; carnauba wax, 7.4 wt %; with 0.03 wt % of stearic acid. The N18 powder solids loading was maintained at 60 vol %, 2–5% below the critical powder loading [1].

The powder was first coated with stearic acid in a vibratory mill, for 30 min and then premixed rotationally with the binder system. A 19 mm twin screw extruder was used for compounding the powder–binder mixture.

To simulate the use of large particle sizes in MIM, a compression moulding machine was used. For compression moulding, discs with a diameter of 50 mm and a thickness range of 4.7–5.5 mm were produced at a mould temperature of 200 °C and compression pressure of approximately 3.7 MPa. After moulding, each compact was cut into smaller test pieces, typically of area 1 cm^2, for the subsequent debinding and sintering. Solvent debinding was carried out using condensed heptane extraction at a temperature of 65 °C followed by a thermal debinding cycle of ramp rate 2 °C min^{-1} to 650 °C, with a subsequent 1 h dwell at 650 °C.

2.3. Die pressing

Discs were produced using a conventional die pressing route. To improve green strength a small amount of binder, consisting of a 3% distilled water solution of polyvinyl alcohol (PVA) and polyethylene glycol (PEG) in the volume ratio of 1 : 3, was mixed with the metal powder in the weight ratio of 1 : 25. Samples were die pressed from the 15–110 μm powder to form 20 mm diameter, 6 mm long pellets using a pressure of 85 MPa. The green density was approximately 60%.

2.4. Sintering

Samples were vacuum sintered. Before sintering, each sample was embedded in an inert boron nitride powder, contained in a pure alumina crucible to provide mechanical support. Heating from ambient temperature was carried out at a ramp rate of 10 °C min^{-1}. Samples were isothermally sintered for 1 h at a range of sintering temperatures between 1150 and 1300 °C. After sintering, the individual samples were measured to determine linear shrinkage, and their final densities were determined using the Archimedes' method.

Samples were examined by optical and scanning electron microscopy (SEM). An image analyser was used to quantify the volume fraction of liquid phase that had been present during sintering by measuring the volume of phases present in the microstructure.

3. Results and discussion

Fig. 2 shows the solidification interval of sintered N18, which occurs over the range 1235–1371 °C according to the cumulative curve of the liquid fraction versus temperature. Compared with the solidification interval of 1225–1323 °C quoted by the powder supplier, the onset of the formation of liquid phase for the solid N18 is approximately 10 °C higher. This result is consistent with

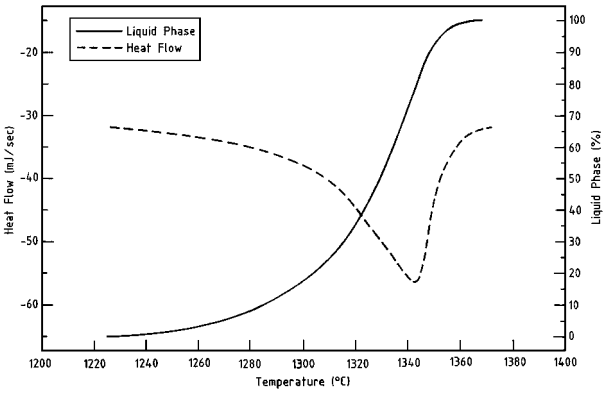

Figure 2 Differential thermal analysis curve of the solidification interval of solid N18, showing the cumulative curve of the liquid volume fraction versus temperature.

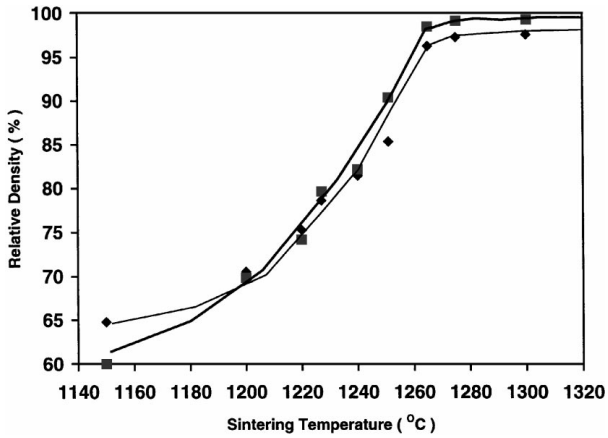

Figure 3 Graph of sintered density versus temperature for samples produced from the MIM processing and die-compaction routes: (♦) die compacted, (■) moulded.

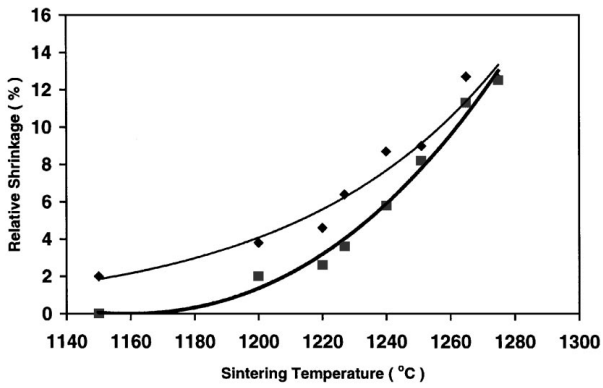

Figure 4 Graph of linear shrinkage versus temperature for samples produced from the MIM processing and die-compaction routes: (♦) die compacted, (■) moulded.

previous studies on other alloys, which have demonstrated that a material in powder form will often exhibit a lower solidus temperature compared with the bulk form due to differences in homogeneity [6].

Figs 3 and 4 compare the sintered densities and linear shrinkages between samples from both the compression moulding and die-pressing routes. They illustrate that the sintering trends are similar for both process routes.

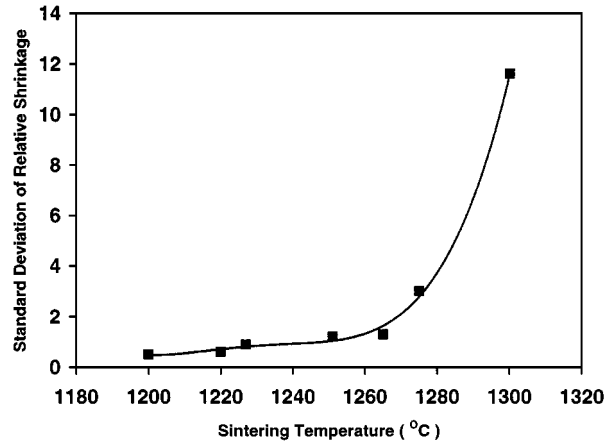

Figure 5 Graph of the standard deviation of specimen shrinkage versus sintering temperature for die-compacted samples.

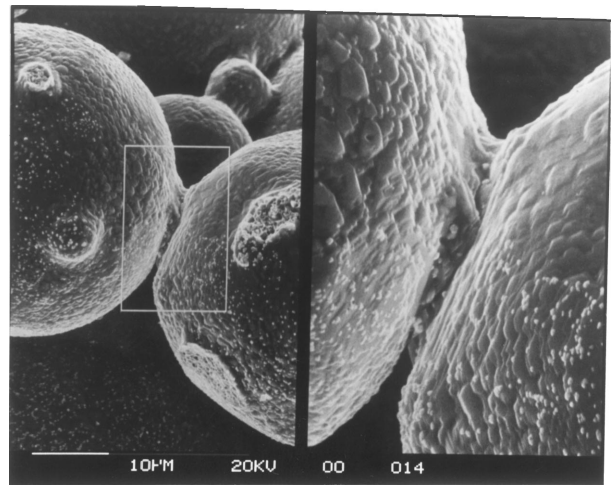

Figure 6 SEM micrograph of N18 powder sintered at 1150 °C for 1 h (the neck formation stage of solid-state sintering can be observed).

The density and shrinkage measurements indicate the onset of significant shrinkage is above 1220 °C, which is indicative of the onset of a liquid phase. This suggests that the solidus temperature of the N18 powder should be located in the vicinity of 1220 °C.

Fig. 3 also indicates that higher densities can be obtained by sintering at higher temperatures. However, as demonstrated in Fig. 5, above 1265 °C the shape-retention of the N18 compacts becomes relatively poor.

Fig. 6 is a secondary electron image of a sample sintered at 1150 °C for 1 h, showing inter-particle neck growth in the absence of liquid phase sintering. Fig. 3 shows that this results in a negligible increase in density over the green density of 60%. Fig. 7 shows optical micrographs of die pressed samples sintered at temperatures between 1250 and 1300 °C for 1 h. Each microstructure shows evidence of SLPS, in the form of a grain-boundary phase. From the microstructures, it is apparent that the compacts sintered at 1275 and 1300 °C exhibit a larger fraction of liquid phase at sintering temperature compared to those processed at 1250 and 1265 °C. This is consistent with liquid volume fraction increasing with temperature. The liquid volume fraction originally present at the different sintering

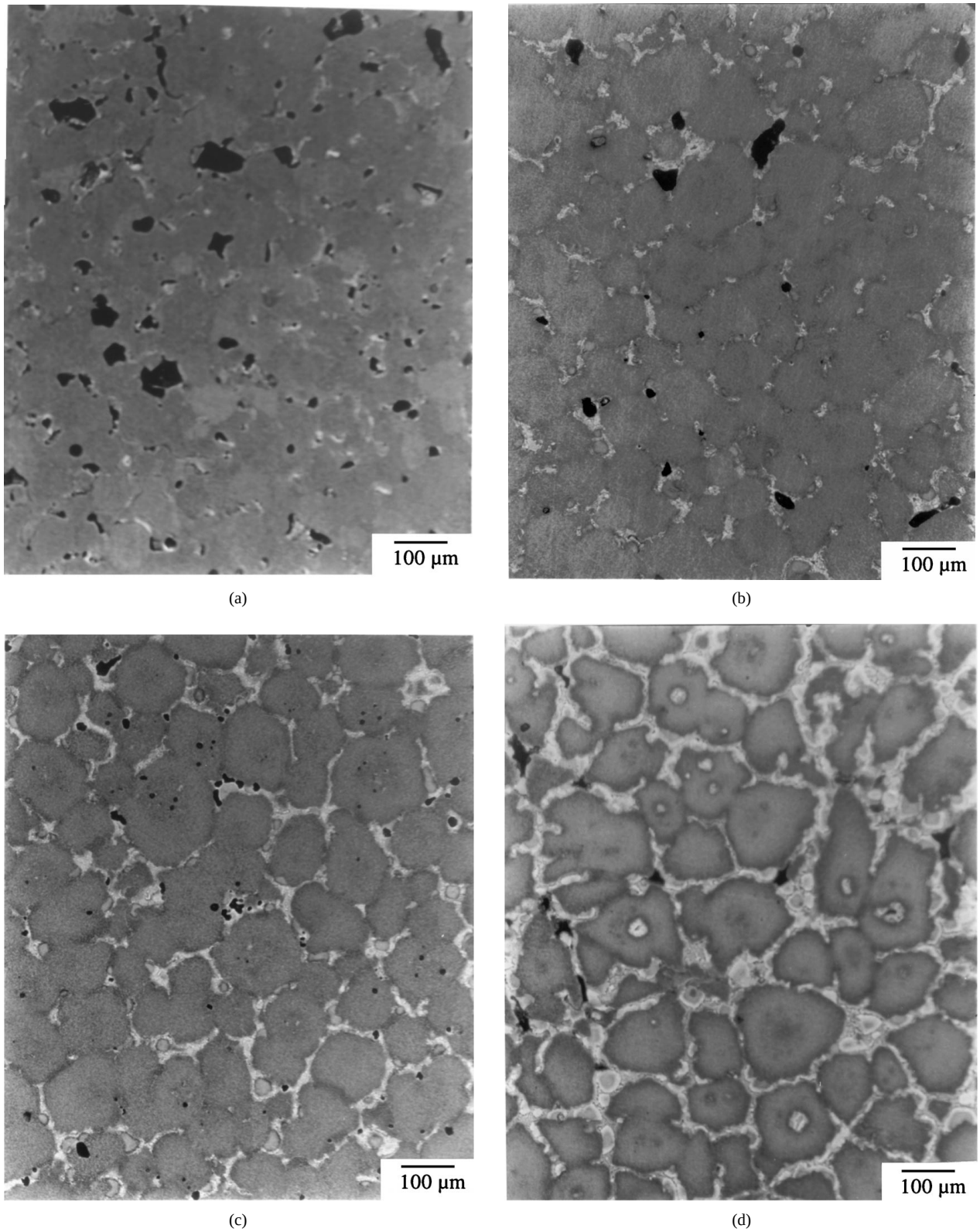

Figure 7 Optical micrographs of SLPS N18 die-pressed samples. Sintering time 1 h. Sintering temperatures: (a) 1250 °C, (b) 1265 °C, (c) 1275 °C, and (d) 1300 °C.

temperatures was estimated from the microstructure using image analysis and is shown in Fig. 8. It is logical to assume that the large liquid volume fraction formed at higher sintering temperatures contributes to the distortion of the compacts during SLPS. Comparison of the results presented in Figs 2 and 8 indicates a reduction in solidus temperature of about 15 °C for the N18 powder, giving a value consistent with that quoted by the powder supplier.

Fig. 9 correlates the sintered densities (Fig. 3) and level of distortion (Fig. 5) with the liquid volume fractions produced at different sintering temperatures for 1 h (Fig. 8). The 0% liquid volume fraction corresponds to the sintered density achieved at 1220 °C for 1 h. This

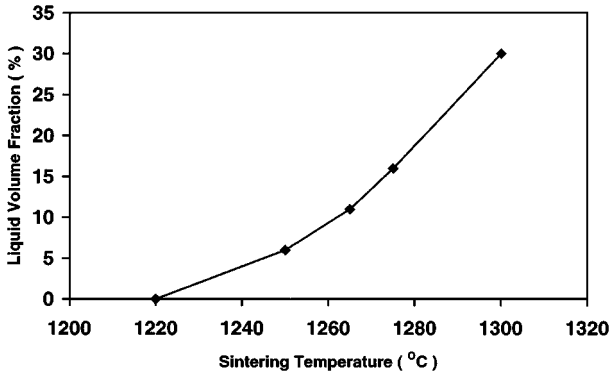

Figure 8 Graph of liquid volume fraction versus sintering temperature for N18 samples calculated from image analysis of the micrographs in Fig. 7.

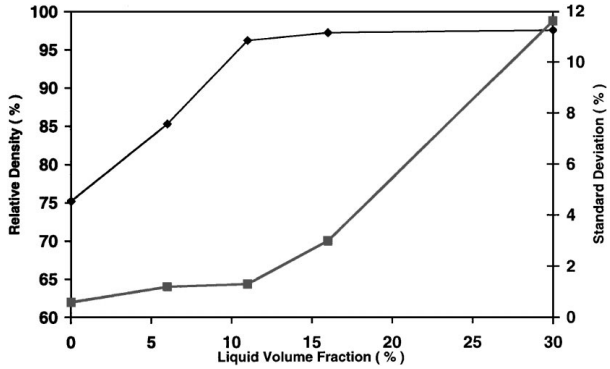

Figure 9 Graph of sintered density versus the liquid volume fraction produced during SLPS. 0% liquid corresponds to the sintered density at 1220 °C for 1 h: (♦) sintered density, (■) standard deviation.

demonstrates that for enhanced densification and minimum distortion a liquid volume fraction of 11% for the SLPS of N18 is about optimum.

Previous investigations of the optimum liquid volume fraction for Ni-base superalloys, such as Astroloy and René 95 [7, 8] ($< 250\,\mu$m powder size), indicated that a higher liquid volume fraction would be required for optimum sintering. Such differences could be due to variations in particle sizes and initial powder microstructure. The N18 powder particles possess a cellular microstructure, which assists in the formation of a continuous liquid film along the grain boundaries, thus reducing the amount of liquid phase required for optimum densification.

The effect of hold time, at the optimum sintering temperature of 1265 °C, on the final density is illustrated in Fig. 10. The density for a sintering time of zero minutes was obtained by furnace cooling the sample immediately after the sintering temperature of 1265 °C had been reached. Fig. 10 suggests that densification occurs predominantly during the first 10–30 min and a longer dwell only marginally improves the final density. A maximum density of 98.5% of theoretical was achieved after 90 min, whereas a density of 94% was achieved after 40 min. Similar observations for Ni-base superalloys Astroloy and René 95 have been reported by Jeandin *et al.* [8]. The sintering kinetics are consistent with the three established super-solidus liquid-phase sintering stages whereby liquid flow provides

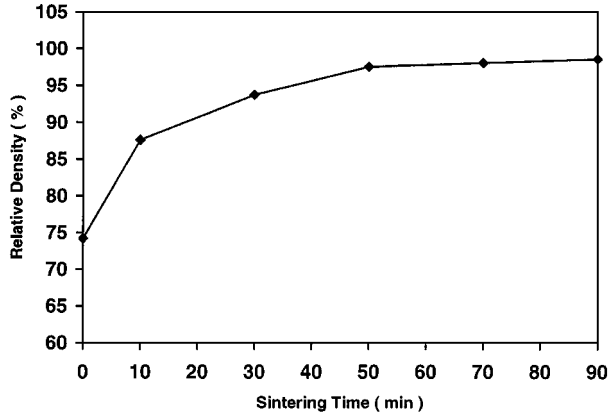

Figure 10 Graph of the sintered density versus the sintering time at 1265 °C for die-compacted samples.

rapid viscous flow-induced densification, a solution and reprecipitation mechanism leads to further densification, and finally solid-state sintering gives rise to a relatively minor increase in final density.

In summary, the sintered densities of the compacts in this study indicate that high densities can be obtained by using coarse pre-alloyed powders combined with SLPS at an optimal sintering temperature.

The slight difference in the sintering behaviour between samples produced by die-pressing and compression moulding routes is shown in Figs 3 and 4. These small differences can be explained by slightly different initial green densities and particle size distributions used for both processing routes and from sample to sample. Nevertheless, the high sintered densities, obtained by SLPS following the moulding process, are comparable with those by SLPS following die pressing. This implies that the moulding route combined with SLPS for mass-producing complex and near-net-shape components from coarse powders is technically feasible.

4. Conclusions

Plastic forming processes in conjunction with SLPS enable large particle sizes of 40–63 μm pre-alloyed powder to be used for the production of components that sinter to a high density. A similar binder formulation to conventional MIM, consisting of polypropylene, paraffin wax, carnauba wax and stearic acid, has been successfully utilized in this study. Solid-state sintering of the coarse powder results in a low final density of the component, typically 61% theoretical density at a sintering temperature of 1150 °C for 1 h. However, with SLPS, densities in excess of 98% can be achieved.

For N18 powder, a minimum liquid volume fraction of 11% is required to achieve 96% theoretical density. Higher densities can be achieved with a higher volume fraction of the liquid phase. However, the need to minimize distortion requires a compromise between good dimensional control and accelerated sintering. Sintering at 1265 °C for 1 h gives the optimum combination of density and acceptable dimensional control.

References

1. R. M. GERMAN, in "Powder Injection Molding" (MPIF, NJ, 1990).
2. *Idem, Int. J. Powder Metall*. **26** (1990) 23.
3. *Idem, ibid*. **23** (1987) 237.
4. C. DUCROCQ, A. LASALMONIE and Y. HONNORAT, in Proceedings of the Sixth International Symposium on Superalloys (Superalloys 1988), Champion, PA, September 1988, edited by D. N. Duhl (Metallurgical Society of AIME, Warrendale PA, 1988) p. 63.
5. K. F. HENS, S. T. LIN, R. M. GERMAN and D. LEE, *J. Metall*. **41** (1989) 17.
6. P. F. MURLEY and R. M. GERMAN, in "1989 Advances in Powder Metallurgy," Vols 1–3, edited by T. G. Gasbarre and W. F. Jandeska (Metal Powder Industries Federation, NJ, 1989) p. 103.
7. M. JEANDIN, J. L. KOUTNY and Y. BIENVENU, *Powder Metall*. **26** (1983) 17.
8. M. JEANDIN, S. RUPP, J. MASSOL and Y. BIENVENU, *Mater. Sci. Eng*. **77** (1986) 139.

Received 1 June
and accepted 4 August 1998